Diagnosing the Ice Crystal Enhancement Factor in the Tropics

Xiping Zeng[1,2], Wei-Kuo Tao[2], Toshihisa Matsui[1,2], Shaocheng Xie[3], Stephen Lang[2,4], Minghua Zhang[5], David O'C Starr[2], Xiaowen Li[1,2], and Joanne Simpson[2]

[1]Goddard Earth Sciences and Technology Center, University of Maryland at Baltimore County, Baltimore, Maryland

[2]Laboratory for Atmospheres, NASA Goddard Space Flight Center, Greenbelt, Maryland

[3]Atmospheric Sciences Division, Lawrence Livermore National Laboratory, Livermore, California

[4]Science Systems and Applications Inc., Lanham, Maryland

[5]School of Marine and Atmospheric Sciences, Stony Brook University, New York

Submitted to *Journal of the Atmospheric Sciences*

June 9, 2009

Corresponding author address: Dr. Xiping Zeng, C423, Bldg 33, Mail Code 613.1, NASA Goddard Space Flight Center, Greenbelt, MD 20771. Email: Xiping.Zeng-1@nasa.gov

Abstract

Recent modeling studies have revealed that ice crystal number concentration is one of the dominant factors in the effect of clouds on radiation. Since the ice crystal enhancement factor and ice nuclei concentration determine the concentration, they are both important in quantifying the contribution of increased ice nuclei to global warming. In this study, long-term cloud-resolving model (CRM) simulations are compared with field observations to estimate the ice crystal enhancement factor in tropical and mid-latitudinal clouds, respectively. It is found that the factor in tropical clouds is $\sim 10^3$-10^4 times larger than that of mid-latitudinal ones, which makes physical sense because entrainment and detrainment in the Tropics are much stronger than in middle latitudes. The effect of entrainment/detrainment on the enhancement factor, especially in tropical clouds, suggests that cloud microphysical parameterizations should be coupled with subgrid turbulence parameterizations within CRMs to obtain a more accurate depiction of cloud-radiative forcing.

1. Introduction

Clouds affect the global energy cycle via radiation (Charney 1979; Hartmann *et al.* 1992) and therefore provide a platform for cloud microphysics to significantly impact climate change (National Research Council 2005; Zeng et al. 2009a). The ice crystal enhancement factor, defined as the ratio of ice crystal concentration to ice nuclei (IN) concentration, varies from one cloud to another (Pruppacher and Klett 1997). Since the factor is important in modeling clouds and radiation (Zeng et al. 2008, 2009b), knowing its climatological characteristics (e.g., ensemble average, geographic distribution) is imperative for quantifying the contribution of increased IN to global warming. In this paper, long-term cloud-resolving model (CRM) simulations are compared with field observations to infer the ice crystal enhancement factor at different latitudes.

a. Ice crystal multiplication

Ice crystal multiplication in clouds is still perplexing. Ice crystal number concentrations often exceed IN concentrations estimated at the cloud-top temperature by up-to four orders of magnitude (e.g., Koenig 1963; Mossop et al. 1968; Mossop 1985; Hobbs and Rangno 1985, 1990; Blyth and Latham 1993). A riming-splintering mechanism, identified by Hallett and Mossop (1974), is one candidate for high ice crystal multiplication (Blyth and Latham 1997; Phillips et al. 2001). This mechanism works when cloud temperatures are between -3 and -8°C and large droplets (≥24 μm diameter) as well as relatively fast falling (0.7 m/s) ice particles are present (e.g., Hallett and Mossop 1974; Mossop 1985). The mechanism, owing to its strict conditions, cannot be used to explain high ice crystal multiplication directly.

Blyth and Latham (1997), based on field observations, proposed a multi-thermal model of cloud glaciation and revealed that the riming-splintering mechanism contributes significantly to ice crystal multiplication via fine cloud dynamical structure. Using a three-dimensional (3D) high-resolution cloud model, Ovtchinnikov et al. (2000) explicitly simulated the fine dynamic structure and confirmed its importance in ice crystal multiplication.

Due to the effects of fine-scale cloud dynamics on microphysics, a CRM with a horizontal resolution of ~1 km must be re-evaluated. Since the model cannot represent fine cloud dynamical structure explicitly, it cannot properly simulate ice crystal multiplication if no corresponding parameterization is introduced. Hence, it is of interest to parameterize the ice crystal multiplication in a CRM.

b. Entrainment and detrainment in tropical clouds

Fine cloud dynamical structure has been explored from aircraft observations (e.g., Malkus and Scorer 1955; Warner 1970; Paluch 1979; Blyth et al. 1988; Damiani et al. 2006). Updrafts usually take the form of entraining and detraining thermals, and the mixing between a thermal and its surrounding air takes place as a series of discrete events rather than continuously (e.g., Austin et al. 1985; Damiani et al. 2006). Since the mixed thermals eventually move to the level of zero buoyancy (Raymond and Blyth 1986; Taylor and Baker 1991; Emanuel 1994), mixing dominates the fine dynamical structure in clouds and therefore affects ice crystal multiplication.

However, the mixing varies greatly from one geographic region to another. Frequent downdrafts, for example, have been observed in the Tropics but not in middle latitudes

(e.g., Heymsfield et al. 1978; Wei et al. 1998; Igau et al. 1999). After reviewing the aircraft observations from over the past decades, Zipser (2003) concluded that undilute updraft cores have not been found in the Tropics but are common in severe storms in middle latitudes. Based on this meridional variation in fine cloud dynamic structure, it is inferred that the ice crystal enhancement factor in the Tropics is much larger than that in middle latitudes (see Sec. 4.a for more discussion). Such variation, in the absence of direct observations, can be verified with cloud observations via CRM simulations.

c. Field observations and CRM simulations

Recent CRM simulations have revealed that cloud ensembles and radiation are sensitive to the ice crystal enhancement factor (Zeng et al. 2008, 2009b). Suppose that a CRM is assigned different ice crystal enhancement factors for different simulations. If a cloud simulation can be made to match the associated observations, then its assigned enhancement factor should be a better inference of the *in-situ* enhancement factor. This diagnostic approach (see Sec. 2 for details) can be applied to estimate the enhancement factor over various geographic regions, with the aid of field campaign observations.

Three field campaigns have provided high-quality cloud observations as well as the corresponding large-scale forcing: the Tropical Warm Pool – International Cloud Experiment (TWP-ICE), the Kwajalein Experiment (KWAJEX) and the Atmospheric Radiation Measurement program's Spring 2000 Cloud field campaign conducted at the Southern Great Plains (ARM-SGP). Comparing the cloud observations from the three campaigns with CRM simulations, the ice crystal enhancement factor over those regions can be estimated and further analyzed to determine how it varies meridionally.

The present study investigates the meridional variation in ice crystal enhancement factor. It consists of five sections. In Sec. 2, a CRM is described with special attention on how to represent IN and ice crystal enhancement factor. In Sec. 3, CRM simulations over three geographic regions are carried out and their results compared with observations to infer the ice crystal concentrations in each region. In Sec. 4, a theoretical model is introduced connecting the ice crystal enhancement factor and fine cloud dynamic structure, which is then used to explain the meridional variation in the enhancement factor. Section 5 concludes.

2. Experiment setup

A 3D CRM, the Goddard Cumulus Ensemble (GCE) model (Tao and Simpson 1993; Tao *et al.* 2003), is used to simulate clouds and radiation. The model is non-hydrostatic and anelastic. It takes account of both absorption and scattering for solar radiation and both emission and absorption for infrared radiation. Its cloud-radiation interaction has been assessed (Tao *et al.* 1996). The model parameterizes subgrid-scale (turbulent) processes with a scheme based on Klemp and Wilhelmson (1978) and Soong and Ogura (1980) and incorporates the effects of both dry and moist processes on the generation of subgrid-scale kinetic energy. The model uses a three-class ice formulation based on Rutledge and Hobbs (1984) with some modifications (Lang et al. 2007; Zeng et al. 2008) for cloud microphysics. It includes the sedimentation of cloud ice (Starr and Cox 1985) to better simulate clouds in the upper troposphere. It calculates all scalar variables (temperature, water vapor, and all hydrometeors) with a positive definite advection scheme (Smolarkiewicz and Grabowski 1990).

All of the numerical experiments in this study follow the model setup used in previous studies (e.g., Johnson *et al.* 2002; Xie *et al.* 2005; Xu *et al.* 2005; Blossey *et al.* 2007; Zeng *et al.* 2007), which simulated clouds with prescribed large-scale forcing derived from field observations. The experiments are 3D, using a 1 km horizontal resolution and a vertical resolution that ranges from 42.5 m at the bottom to 1 km at the top. The model uses 256 x 256 x 41 gridpoints and a time step of 6 seconds for integration. Other model parameters are detailed in Zeng et al. (2008, 2009b).

The model has five prognostic hydrometeor variables: the mixing ratios of cloud water, rainwater, cloud ice, snow and graupel. It parameterizes the Bergeron process via the IN concentration and ice crystal enhancement factor. The conversion rate of cloud ice to snow due to vapor deposition is expressed as (Zeng et al. 2008, 2009b)

$$\max\left[2a_1(3q_i - m_{I50}\rho^{-1}\mu N_i)m_{I50}^{a_2-1}, 0\right], \tag{2.1}$$

and the conversion rate of cloud water to ice as

$$\frac{2}{(a_2+1)(a_2+2)}\left[3a_2 q_i + (1-a_2)m_{I50}\rho^{-1}\mu N_i\right]a_1 m_{I50}^{a_2-1}, \tag{2.2}$$

where N_i is the number concentration of active ice nuclei, q_i the mixing ratio of cloud ice, a_1 and a_2 the temperature-dependent parameters in the Bergeron process (Koenig 1971), ρ the air density, m_{I50}=4.8×10^{-7} g the mass of an ice crystal 50 μm in diameter, and the parameter μ represents the ice particle enhancement factor due to riming-splintering and other mechanisms (Hallet and Mossop 1974).

The model uses the formula of Fletcher (1962) to compute the active IN concentration in clouds as a function of air temperature T or

$$N_i = n_0 \exp\left[\beta(T_0 - T)\right] \tag{2.3}$$

where n_0 and β are constant. To explore the effects of IN and ice crystal multiplication on clouds and radiation, different IN concentrations and ice crystal enhancement factors are tested for each large-scale forcing. Table 1 shows the six categories of ice crystal concentration used in the numerical simulations. Generally speaking, ice crystal concentration increases as the crystal concentration category changes from I to VI.

Since there were no *in-situ* observations of IN concentration and ice crystal enhancement factor in the three field campaigns, *in-situ* IN concentrations and crystal enhancement factor are implied by comparing CRM simulations with field observations. If a CRM simulation with specific values of μn_0 and β agrees well with field observations (i.e., radar, satellite, sounding networks and other measurements), then those values are treated as the *in-situ* ones.

3. Diagnosing the ice crystal concentrations

In this section, CRM simulations over three geographic regions are carried out and their results compared with cloud observations to diagnose the ice crystal concentrations (or the products of IN concentration and ice crystal enhancement factor) in each region. The simulations are summarized in Table 2.

a. TWP-ICE simulations

To model the tropical clouds observed in TWP-ICE, three simulations T06L, T06M and T06H are carried out using the crystal concentration categories II, IV and V (see Table 1 for definition), respectively. Obviously, the three simulations correspond to low, moderate and high ice crystal concentrations, respectively. Next, their results are

compared with TWP-ICE observations to determine which category of crystal concentration brings about reasonable results.

TWP-ICE was conducted in Darwin, Australia in January and February of 2006 during the northern Australian monsoon season (May et al. 2008). It was centered at (12°S, 131°E). It provided a great deal of information on clouds such as the liquid and ice water contents obtained from ARM Micro-base products (Miller *et al.* 2003). It also provided the large-scale forcing data (e.g., vertical motion and horizontal advective tendencies of temperature and moisture) derived using the variational analysis approach described in Zhang and Lin (1997) and Zhang *et al.* (2001). The large-scale forcing data represent the mean domain with a center at (12°S, 131°E) and a radius of ~120 km (see Xie et al. 2009 for more details of the forcing). The present study focuses on the period from 2100 UTC 6 to 12 February 2006, a typical monsoon break period, during which convection was characterized by intense afternoon thunderstorms with several squall lines crossing Darwin in the evening and early morning.

All three simulations start at 2100 UTC 6 February 2006 and last for 6 days. Figure 1 displays the three-hour averages of precipitation rate in the simulations. It also displays the observed precipitation rate for comparison. Generally speaking, the model captured the main precipitation events in spite of some quantitative deviations. The figure also shows that the ice crystal concentration can obviously affect precipitation (e.g., day 1.5, 3, 4.5, 5.1 and 5.8).

Moreover, as the ice crystal concentration increases from low to moderate to high, the modeled average precipitation rate decreases while the modeled average precipitable water amount increases from 51.5 to 52.5 mm. Compared to the observed precipitable

water amount of 54.7 mm, the high ice crystal concentration brings about the most reasonable amount of precipitable water, which is consistent with previous results for GATE (the Global Atmospheric Research Program's Atlantic Tropical Experiment) simulations (Zeng et al. 2009b).

In addition, the ice crystal concentration can affect cloud ensembles significantly. Figures 2 and 3 display time-pressure cross sections of the simulated ice contents using the low and high crystal concentrations, respectively. The two figures show that cloud ice content in the upper troposphere increases significantly with increasing ice crystal concentration, but snow and graupel do not.

The modeled ice content can be compared with the observed to determine which category of crystal concentration, if any, is close to the *in-situ* concentration. Figure 4 displays the vertical profile of six-day mean ice water content retrieved from the radar observations over the Darwin station. The retrieval algorithm has been well tested on thin non-precipitating clouds but not on thick precipitating clouds (Dong and Mace 2003). Figure 4 also displays the vertical profiles of mean modeled ice content (the sum of the cloud ice, snow and graupel mixing ratios) for comparison. Obviously, the ice profile using the high crystal concentration is close to the retrieved profile above 360 hPa, but those using the low and moderate crystal concentrations are not.

However, all of the modeled ice contents differ greatly from the retrieved below the 360 hPa level. This difference between the retrieved and modeled contents is not just due to model but also the retrieval algorithm. In the retrieval algorithm, it is difficult to distinguish ice from liquid water using radar reflectivity, especially in the mixed-phase region (X. Dong, personal communication, 2008). Hence, the retrieval in the mixed-phase

region may contain a large error and therefore partly explains the difference between the retrieved and modeled ice contents below the 360 hPa level.

Since ice particles, rather than supercooled drops, are common in the upper troposphere (e.g., above the 360 hPa level), the retrieval of ice water content is reliable there (Dong and Mace 2003). Hence, based on the comparison between the modeled and retrieved ice water contents above the 360 hPa level, it is inferred that the ice crystal concentration in the Tropics is high. To support this conclusion on ice crystal concentration, satellite observations are compared with CRM simulations over another tropical region.

b. KWAJEX simulations

In contrast to TWP-ICE, KWAJEX was conducted over a tropical open ocean. It was centered at (8.8°N, 167.4°E) and took place from July 23 through September 15, 1999. Two numerical simulations are carried out to model the clouds observed during KWAJEX. Both simulations start at 0600 UTC 24 July 1999 and last for 52 days. The model setup is the same as that for the TWP-ICE simulations.

The two simulations are driven with large-scale forcing derived using the same variational analysis approach described in Zhang and Lin (1997) and Zhang *et al.* (2001), and the crystal concentration categories II and V, respectively. The first one, K3DN, uses category V and was introduced briefly in Zeng et al. (2008). The second one, K3DL, uses category II and its results resemble experiment K3DD described in Zeng et al. (2008).

K3DN and K3DL correspond to the high and low crystal concentrations, respectively. Their modeled precipitation rate, just as shown in Zeng et al. (2008), decreases while

precipitable water increases with increasing crystal concentration. The modeled variables (e.g., rainfall rate, precipitable water) approach the observed values for the high crystal concentration run. Next, satellite observations are compared with the results to show that the cloud ensembles from the high crystal concentration simulation are close to the observed.

A precipitation radar (PR) was included on the Tropical Rainfall Measuring Mission (TRMM) satellite (Simpson et al. 1988), which flew over the KWAJEX region obtaining vertical profiles of radar reflectivity during the campaign. Figure 5 displays the vertical profiles of mean and maximum radar reflectivity obtained from the TRMM observations over the period. The figure also displays the vertical profiles of simulated radar reflectivity sampled when the satellite flew over the campaign site (see Matsui et al. 2009 for the computational procedure). As shown in the figure, the reflectivity profiles using the high crystal concentration are closer to the observed especially in the upper troposphere.

In summary, both the TWP-ICE and KWAJEX simulations show that the modeled quantities (i.e., upper-tropospheric cloud ensembles, precipitable water, and precipitation rate) are closer to the observed for the *high* crystal concentration. Simulations over other tropical regions [e.g., GATE and SCSMEX (the South China Sea Monsoon Experiment)] also support this conclusion that the ice crystal concentration is high in the Tropics (Zeng et al. 2008, 2009b).

c. ARM-SGP simulations

Unlike TWP-ICE and KWAJEX, ARM-SGP was centered at (36.6°N, 96.5°W) and thus focused on continental clouds in middle latitudes. One ARM-SGP campaign was conducted in the spring of 2000. Three simulations, A00H, A00M and A00L, are carried out to model the clouds observed during the campaign. All the simulations start at 1730 UTC 1 March 2000 and last for 20 days. Their model setup follows those for the TWP-ICE and KWAJEX experiments except that the surface fluxes are provided by observations.

These experiments with three different ice crystal concentrations (see Table 2 for details) have been analyzed previously in Zeng et al. (2009b). Next, the resulting cloud ensembles are quantitatively compared with the observed to determine the ice crystal concentration during the campaign.

Figure 6, just like Fig. 4, displays the vertical profile of ice water content retrieved from radar observations. The figure also presents the vertical profiles of modeled ice water content from the three simulations. As shown in the figure, the ice water content from the *low* ice crystal concentration is closer to the observed above the 400-hPa level, which indicates that the ice crystal concentration in spring is rather low in middle latitudes.

Similarly, other ARM-SGP simulations (e.g., those for the summer of 1997 and 2002) have shown that the diagnosed ice crystal concentration in summer is quite low in middle latitudes too (Zeng et al. 2009a, b). The critical question is *why is the climatological value of ice crystal concentration for midlatitudinal clouds relatively low but for tropical clouds relatively high*. This issue is addressed next with theoretical analyses and other observations.

4. Meridional variation in the ice crystal enhancement factor

The high ice crystal concentration in tropical clouds is attributed either to a large IN concentration or ice crystal enhancement factor. Since IN are usually generated by natural and human activities over continents (Pruppacher and Klett 1997; DeMott et al. 2003; Möhler et al. 2007; Phillips et al. 2008) and there are no IN observations over the field campaigns, the *in-situ* active IN concentrations there are estimated based on their geographic locations.

TWP-ICE, KWAJEX and ARM-SGP occurred in coastal, oceanic and continental regions, respectively. Generally speaking, the IN concentrations over the first two campaigns should be lower than that over the last. Based on the preceding conclusion that the ice crystal concentrations over the tropical campaigns are much higher than that over the mid-latitudinal one, it is inferred that the ice crystal enhancement factor in the Tropics is much larger than that over middle latitudes, even assuming that the IN concentrations over the three campaigns are close to each other.

The enhancement factor over the tropical campaigns, with the aid of Table 1, is quantitatively compared with that over the mid-latitudinal one. The diagnosed crystal concentration over ARM-SGP is close to crystal concentration category II, whereas those over TWP-ICE and KWAJEX are close to category V. Suppose that the IN concentrations (or N_i) over the three campaigns have the same order of magnitude. Thus, the difference in μN_i between category II and V indicates that the enhancement factor μ over TWP-ICE and KWAJEX is 10^3-10^4 times larger than that over ARM-SGP, which is further explained using a simple theoretical model.

a. A theoretical model

Consider an air parcel with a temperature lower than 0°C and relative humidity of 100% with respect to water. The parcel fluctuates vertically around its original position due to moist turbulence. Let Δz_m denote the maximum vertical displacement of the parcel above its original position. Thus, the ice crystal enhancement factor due to moist turbulence is obtained from Eq. (2.3). That is

$$\mu = \exp(\beta \gamma_s \Delta z_m) \tag{4.1}$$

where γ_s is the saturated adiabatic lapse rate. Obviously, (4.1) takes no account of the ice crystal multiplication due to the riming-splintering mechanism and other multiplication processes.

Expression (4.1) shows that the enhancement factor increases significantly with increasing Δz_m. Suppose β=0.6 and γ_s=7°C/km. Thus, μ=10 when Δz_m=548 m, and μ reaches 10^3 when the vertical displacement is 1.5 km or so.

Convective updrafts and downdrafts, as a part of moist turbulence, can determine the maximum vertical displacement of air parcels. Since the drafts vary in frequency from one geographic region to another, they can bring about a geographic variation in the ice crystal enhancement factor. Aircraft observations show that there are so many downdrafts in the Tropics but not in middle latitudes (e.g., Heymsfield et al. 1978; Wei et al. 1998; Igau et al. 1999). And, undilute updraft cores have not been found in the Tropics but are common in severe storms in middle latitudes (Zipser 2003). Aircraft observations also show that ice crystal concentrations are quite small in updrafts cores but large along the edges and in downdrafts (e.g., Damiani et al. 2006). All of the observations are

consistent with the concept that frequent downdrafts in the Tropics contribute a great deal to the high ice crystal concentration (or crystal enhancement factor) there and therefore support (4.1).

b. Effect of the ice crystal enhancement factor

The present CRM simulations use μN_i to represent ice crystal concentration. Just as shown in (2.3) and (4.1), μ and N_i vary differently with height. Next, a new TWP-ICE simulation is carried out to show whether the enhancement factor and its vertical distribution affect cloud ensembles.

Simulation T06Hu follows the same setup as T06L and T06H except for the ice crystal concentration. Suppose that the IN concentration over TWP-ICE is close to that over ARM-SGP. Thus, the IN concentration in the simulations is calculated with (2.3) using β=0.6 and n_0=1.2×10^{-9} cm^{-3}.

Based on (4.1) and Blyth and Latham (1997), the enhancement factor is approximated with

$$\mu = \mu_0 \exp[\alpha(T - T_0)] \qquad \text{when } T<T_0 \qquad (4.2)$$

where α=0.1 K^{-1} and μ_0 =10^4 are chosen. The enhancement factor in (4.2), which is different from the IN concentration, is larger when an air parcel is closer to the freezing level.

T06Hu differs from T06L and T06H only in crystal concentration. Figure 7 displays the crystal concentrations versus air temperature used in T06Hu, T06L and T06H. The concentration in T06Hu is much higher than that in T06L. It is close to that in T06H in

general but increases with height less fast than in H06H. In brief, T06Hu uses an enhancement factor of ~10^4 and an IN concentration that is close to the ARM-SGP value.

Figure 8 displays time-pressure cross sections of the cloud ice, snow and graupel mixing ratios in the new simulation. It is compared with Fig. 2 to show whether the enhancement factor affects upper-tropospheric ice water content, since T06Hu uses an IN concentration similar to T06L but an enhancement factor of ~10^4. The contrast between the two figures indicates that the large enhancement factor brings about a high ice water content in the upper troposphere.

Figure 9 displays the time-pressure cross section of retrieved ice water content over the Darwin station. Compared with Figs. 2 and 8, it shows that the modeled cloud ice contents in T06Hu as well as in T06H are closer to the retrieved ice water content than that from T06L, indicating that the ice crystal enhancement factor over TWP-ICE is ~10^4.

Contrasting Figs. 8 and 3 reveals the effect of the vertical distribution of the enhancement factor on upper-tropospheric ice water content, because T06Hu and T06H use similar crystal concentrations but different vertical distributions of crystal concentration. In reference to the retrieved ice water content shown in Fig. 9, the modeled cloud ice content in the upper troposphere has a better cloud structure from day 4 to 6 in T06Hu than in T06H, which implies that the vertical distribution of the enhancement factor can significantly affect cloud ensembles and therefore should be determined by a physically-based scheme.

5. Conclusions and discussion

Since both the IN concentration and ice crystal enhancement factor strongly impact upper-tropospheric ice water content (e.g., Zeng et al. 2008, 2009b), they are both important in quantifying the contribution of increased IN to global warming (Zeng et al. 2009a). Due to the sparse cloud sampling by aircraft, no climatological information on the enhancement factor is currently available. In this paper, long-term cloud simulations are compared with field observations to infer a meridional variation in the enhancement factor, which is summarized as follows.

- Long-term CRM simulations are compared with TWP-ICE, KWAJEX and ARM-SGP cloud observations. It is found that the ice crystal enhancement factor in the Tropics is ~10^3-10^4 times larger than that in middle latitudes.
- The significant decrease in the enhancement factor with increasing latitude makes physical sense. Since fine cloud dynamic structure (e.g., convective downdrafts) can affect the enhancement factor greatly and it varies significantly from one geographic region to another, the frequent downdrafts or strong vertical mixing in the Tropics bring about the large enhancement factor there.
- Consider CRMs with a horizontal resolution of ~1 km. Since they do not simulate moist eddies explicitly, they should parameterize the effect of moist eddies on ice crystal concentration. In the present study, CRM simulations with different assigned crystal concentrations are compared with observations to infer (or diagnose) *in-situ* crystal concentrations. It is found that the ice crystal concentration or ice crystal enhancement factor varies significantly with latitude. Hence, to obtain more accurate prediction of cloud radiative forcing in a CRM,

the representation of ice crystal concentration should be coupled with subgrid turbulence parameterization. This is usually overlooked in current CRMs.

Acknowledgements This research was supported by the Office of Science (BER), U. S. Department of Energy/Atmospheric Radiation Measurement (DOE/ARM) Interagency Agreement No. DE-AI02-04ER63755 and -09ER64753. The research was also supported by the NASA Headquarters Atmospheric Dynamics and Thermodynamics Program and the NASA Tropical Rainfall Measuring Mission (TRMM). The authors are grateful to Dr. Kiran Alapaty at DOE/ARM and Dr. R. Kakar at NASA headquarters for their support of this research. The research was also supported by NASA and the DOE Atmospheric Radiation Measurement Program at the Stony Brook University. Dr. Xie, working at LLNL, was supported under the auspices of the U. S. Department of Energy/Office of Science, Biological and Environmental Research by the University of California Lawrence Livermore National Laboratory under contract No. DE-AC52-07NA27344. The authors acknowledge the NASA Ames Research Center and the NASA Goddard Space Flight Center for the computer time used in this research.

References

Austin, P. H., M. B. Baker, A. M. Blyth and J. B. Jensen, 1985: Small-scale variability in warm continental cumulus clouds. *J. Atmos. Sci.*, **42**, 1123-1138.

Blossey, P. N., C. S. Bretherton, J. Cetrone, and M. Kharoutdino, 2007: Cloud-resolving model simulations of KWAJEX: model sensitivities and comparisons with satellite and radar observations. *J. Atmos. Sci.,* **64**, 1488-1508.

Blyth, A. M. and J. Latham, 1993: Influence of glaciation on an effective-radius parameterization. *Quart. J. Roy. Meteo. Soc.*, **119**, 1469-1474.

Blyth, A. M. and J. Latham, 1997: A multi-thermal model of cumulus glaciation via the Hallett-Mossop process. *Quart. J. Roy. Meteor. Soc.*, **123**, 1185-1198.

Blyth, A. M., W. A. Cooper and J. B. Jensen, 1988: A study of the source of entrained air in Montana cumuli. *J. Atmos. Sci.*, **45**, 3944-3964.

Charney, J. G. 1979: *Carbon Dioxide and Climate: A Scientific Assessment*. Nat. Acad. Sci., Washington, DC. 22 pp.

Damiani, R., G. Vali, and S. Haimov, 2006: The structure of thermals in cumulus from airborne dual-Doppler radar observations. *J. Atmos. Sci.*, **63**, 1432-1450.

DeMott, P. J. and Coauthors, 2003: Measurements of the concentration and composition of nuclei for cirrus formation. *PNAS*, **100**, 14655-14660.

Dong, X., and G. G. Mace, 2003: Profiles of low-level stratus cloud microphysics deduced from ground-based measurements. *J. Atmos. Oceanic Tech.*, **20**, 42-53.

Emanuel, K. A., 1994: *Atmospheric Convection*. Oxford University Press, New York, 580pp.

Fletcher, N. H., 1962: *The physics of Rain Clouds*. The Cambridge University Press, 386 pp.

Hallett, J., and S. C. Mossop, 1974: Production of secondary ice particles during the riming process. *Nature*, **249**, 26-28.

Hartmann, D. L., M. E. Ockert-Bell and M. L. Michelsen, 1992: The effect of cloud type on Earth's energy balance: global analysis. *J. Climate*, **5**, 1281-1304.

Heymsfield, A. J., P. N. Johnson and J. E. Dye, 1978: Observations of moist adiabatic ascent in northeast Colorado cumulus congestus clouds. *J. Atmos. Sci.*, **35**, 1689-1703.

Hobbs, P. V., and A. L. Rangno, 1985: Ice particle concentrations in clouds. *J. Atmos. Sci.,* **42,** 2523–2549.

Hobbs, P. V., and A. L. Rangno, 1990: Rapid development of high ice particle concentrations in small polar maritime clouds. *J. Atmos. Sci.,* **47,** 2710–2722.

Igau, R. C., M. A. LeMone, and D. Wei, 1999: Updraft and downdraft cores in TOGA COARE: Why so many buoyant downdraft cores? *J. Atmos. Sci.*, **56**, 2232-2245.

Johnson, D. E., W.-K. Tao, J. Simpson, and C.-H. Sui, 2002: A study of the response of deep tropical clouds to large-scale thermodynamic forcing. Part I: Modeling strategies and simulations of TOGA COARE convective systems. *J. Atmos. Sci.*, **59**, 3492-3518.

Klemp, J. B. and R. B. Wilhelmson, 1978: The simulation of three-dimensional convective storm dynamics. *J. Atmos. Sci.*, **35**, 1070-1096.

Koening, L. R., 1963: The glaciating behavior of small cumulonimbus clouds. *J. Atmos. Sci.*, **20**, 29-47.

Koenig, L. R., 1971: Numerical modeling of ice deposition. *J. Atmos. Sci.*, **28**, 226-237.

Lang, S., W.-K. Tao, R. Cifelli, W. Olson, J. Halverson, S. Rutledge, and J. Simpson, 2007: Improving simulations of convective systems from TRMM LBA: Easterly and westerly regimes. *J. Atmos. Sci.*, **64**, 1141-1164.

Malkus, J. S. and R. S. Scorer, 1955: The erosion of cumulus towers. *J. Meteor.*, **12**, 43-57.

Matsui, T., X. Zeng, W.-K. Tao, H. Masunaga, W. S. Olson, and S. Lang, 2009: Evaluation of long-term cloud-resolving model simulations using satellite radiance observations and multi-frequency satellite simulators. *J. Atmos. Oce. Tech.* (in press).

May, P. T., J. H. Mather, G. Vaughan, C. Jakob, G. M. McFarquhar, K. N. Bower, and G. G. Mace, 2008: The tropical warm pool international cloud experiment. *Bull. Amer. Meteor. Soc.*, **89**, 629-645.

Miller, M. A., K. L. Johnson, D. T. Troyan, E. E. Clothiaux, E. J. Mlawer, and G. G. Mace, 2003: ARM value-added cloud products: Description and status. Thirteenth ARM Science Team Meeting Proceedings, U. S. Dept of Energy, Washington, D. C. (Available from http://www.arm.gov/publications/proceedings/conf13/extended_abs/miller-ma.pdf.)

Möhler, O., P. J. DeMott, G. Vali, and Z. Levin, 2007: Microbiology and atmospheric processes: the role of biological particles in cloud physics. *Biogeosciences*, **4**, 1059-1071.

Mossop, S. C., R. E. Ruskin, and K. J. Heffernan, 1968: Glaciation of cumulus at approximately 4°C. J. *Atmos. Sci.*, **25**, 889-899.

Mossop, S. C., 1985: Secondary ice particle production during rime growth: the effect of drop size distribution and rimer velocity. *Q. J. R. Meteorol. Soc.,* **111**, 1113–1124.

National Research Council, 2005: *Radiative forcing of climate change: expanding the concept and addressing uncertainties*. Nat. Acad. Sci., Washington, DC. 224pp.

Ovtchinnikov, M., Y. L. Kogan, and A. M. Blyth, 2000: An investigation of ice production mechanisms in small cumuliform clouds using a 3D model with explicit microphysics. Part II: Case study of New Mexico cumulus clouds. *J. Atmos. Sci.,* **57**, 3004-3020.

Paluch, I. R., 1979: The entrainment mechanism in Colorado cumuli. *J. Atmos. Sci.*, **36**, 2467-2478.

Phillips, V. T. J., A. M. Blyth, T. W. Choularton, P. R. A. Brown, and J. Latham, 2001: The glaciation of a cumulus cloud over New Mexico. *Quart. J. Roy. Meteor. Soc.*, **127**, 1513–1534.

Phillips, V. T. J., P. J. DeMott, and C. Andronache, 2008: An empirical parameterization of heterogeneous ice nucleation for multiple chemical species of aerosol. *J. Atmos. Sci.* **65**, 2757-2783.

Pruppacher, H. R., and J. D. Klett, 1997: *Microphysics of clouds and precipitation.* Kluwer, 954 pp.

Raymond, D. J. and A. M. Blyth, 1986: A stochastic mixing model for nonprecipitating cumulus clouds. *J. Atmos. Sci.*, **43**, 2708-2718.

Rutledge, S. A. and P. V. Hobbs, 1984: The mesoscale and microscale structure and organization of clouds and precipitation in mid-latitude clouds. Part XII: A diagnostic modeling study of precipitation development in narrow cold frontal rainbands. *J. Atmos. Sci.*, **41**, 2949-2972.

Simpson, J., R. F. Adler and G. R. North, 1988: A proposed Tropical Rainfall Measuring Mission (TRMM) satellite. *Bull. Amer. Meteor. Soc.*, **69**, 278-295.

Smolarkiewicz, P. K., and W. W. Grabowski, 1990: The multidimensional positive advection transport algorithm: non-oscillatory option. *J. Comp. Phys.*, **86**, 355-375.

Soong, S.-T. and Y. Ogura, 1980: Response of tradewind cumuli to large-scale processes. *J. Atmos. Sci.*, **37**, 2035-2050.

Starr, D. O., and S. K. Cox, 1985: Cirrus clouds. Part I: cirrus cloud model. *J. Atmos. Sci.*, **42**, 2663-2681.

Tao, W.-K. and J. Simpson, 1993: The Goddard Cumulus Ensemble model. Part I: Model description. *Terr. Atmos. Oceanic Sci.*, **4**, 19-54.

Tao, W.-K., S. Lang, J. Simpson, C.-H. Sui, B. Ferrier, and M.-D. Chou, 1996: Mechanisms of cloud-radiation interaction in the Tropics and midlatitudes. *J. Atmos. Sci.*, **53**, 2624-2651.

Tao, W.-K., J. Simpson, D. Baker, S. Braun, M.-D. Chou, B. Ferrier, D. Johnson, A. Khain, S. Lang, B. Lynn, C.-L. Shie, D. Starr, C.-H. Sui, Y. Wang and P. Wetzel, 2003: Microphysics, radiation and surface processes in the Goddard Cumulus Ensemble (GCE) model. *Meteor. Atmos. Phys.*, **82**, 97-137.

Taylor, G. R. and M. B. Baker, 1991: Entrainment and detrainment in cumulus clouds. *J. Atmos. Sci.*, **48**, 112-121.

Warner, J., 1970: The microstructure of cumulus clouds. Part III: the nature of the updrafts. *J. Atmos. Sci.*, **27**, 682-688.

Wei, D., A. M. Blyth, and D. J. Raymond, 1998: Buoyancy of convective clouds in TOGA COARE. *J. Atmos. Sci.*, **55**, 3381-3391.

Xie, S., M. H. Zhang, M. Branson, R. T. Cederwall, A. D. Del Genio, Z. A. Eitzen, S. J. Ghan, S. F. Iacobellis, K. L. Johnson, M. Khairoutdinov, S. A. Klein, S. K. Krueger, W. Lin, U. Lohmann, M. A. Miller, D. A. Randall, R. C. J. Somerville, Y. C. Sud, G. K. Walker, A. Wolf, X. Wu, K.-M. Xu, J. J. Yio, G. Zhang and J. Zhang, 2005: Simulations of midlatitude frontal clouds by single-column and cloud-resolving models during the Atmospheric Radiation Measurement March 2000 cloud intensive operational period. *J. Geophys. Res.*, **110**. D15S03, doi:10.1029/2004JD005119.

Xie, S., T. Hume, C. Jakob, S. A. Klein, R. McCoy, and M. Zhang, 2009: Observed large-scale structures and diabatic heating and drying profiles during TWP-ICE. *J. Climate*, (in revision).

Xu, K.-M., M. H. Zhang, Z. A. Eitzen, S. J. Ghan, S. A. Klein, X. Wu, S. Xie, M. Branson, A. D. Del Genio, S. F. Iacobellis, M. Khairoutdinov, W. Lin, U. Lohmann, D. A. Randall, R. C. J. Somerville, Y. C. Sud, G. K. Walker, A. Wolf, J. J. Yio and J. Zhang, 2005: Modeling springtime shallow frontal clouds with cloud-resolving and single-column models. *J. Geophys. Res.*, **110**. D15S04, doi:10.1029/2004JD005153.

Zeng, X., W.-K. Tao, M. Zhang, C. Peters-Lidard, S. Lang, J. Simpson, S. Kumar, S. Xie, J. L. Eastman, C.-L. Shie and J. V. Geiger, 2007: Evaluating clouds in long-term cloud-resolving model simulations with observational data. *J. Atmos. Sci.*, **64**, 4153-4177.

Zeng, X., W.-K. Tao, S. Lang, A. Y. Hou, M. Zhang, and J. Simpson, 2008: On the sensitivity of atmospheric ensembles to cloud microphysics in long-term cloud-resolving model simulations. *J. Meteor. Soc. Japan*, **86A**, 45-65.

Zeng, X., W.-K. Tao, M. Zhang, A. Y. Hou, S. Xie, S. Lang, X. Li, D. Starr, and X. Li, 2009a: A contribution by ice nuclei to global warming. *Quart. J. Roy. Meteor. Soc.* in press, DOI: 10.1002/qj.449.

Zeng, X., W.-K. Tao, M. Zhang, A. Y. Hou, S. Xie, S. Lang, X. Li, D. Starr, X. Li, and J. Simpson, 2009b: An indirect effect of ice nuclei on atmospheric radiation. *J. Atmos. Sci.*, **66**, 41-61.

Zhang, M. H. and J. L. Lin, 1997: Constrained variational analysis of sounding data bases on column-integrated budgets of mass, heat, moisture, and momentum: Approach and application to ARM measurements. *J. Atmos. Sci.*, **54**, 1503-1524.

Zhang, M. H., J. L. Lin, R. T. Cederwall, J. J. Yio, and S. C. Xie, 2001: Objective analysis of ARM IOP Data: Method and sensitivity. *Mon. Wea. Rev.*, **129**, 295-311.

Zipser, E. J., 2003: Some view on "hot towers" after 50 years of tropical field programs and two years of TRMM data. Cloud systems, hurricanes, and the Tropical Rainfall Measuring Mission (TRMM). W.-K. Tao and R. Adler Ed., *Meteor. Monogr.*, **29**, 49-58.

Table 1 Crystal concentration categories used in numerical simulations

Category	μn_0 (cm^{-3})	β
I	6.0×10^{-10}	0.3
II	1.2×10^{-9}	0.4
III	4.8×10^{-9}	0.45
IV	1.2×10^{-8}	0.5
V	1.2×10^{-6}	0.6
VI	1.2×10^{-5}	0.7

Table 2 A list of all the numerical simulations

Field Campaign	*Numerical Experiment*	n_0 (cm^{-3})	β	μ	*Ice Crystal Concentration*	*Close to Observations*
TWP-ICE	T06H	10^{-6}	0.6	1.2	High	Yes
	T06M	10^{-8}	0.5	1.2	Moderate	No
	T06L	10^{-9}	0.4	1.2	Low	No
	T06Hu	1.2×10^{-9}	0.6	Eq. (4.2)	High (see text)	Yes
KWAJEX	K3DN	10^{-6}	0.6	1.2	High	Yes
	K3DL	10^{-9}	0.4	1.2	Low	No
ARM-SGP	A00H	10^{-6}	0.6	1.2	High	No
	A00M	10^{-8}	0.5	1.2	Moderate	No
	A00L	10^{-9}	0.4	1.2	Low	Yes

Caption

Fig. 1 Time series of surface precipitation rate for the TWP-ICE observations and three simulations that start at 2100 UTC 6 February 2006. Thick line represents the observations. Dashed, dot-dashed and dotted lines represent the modeling results with low (T06L), moderate (T06M) and high ice crystal concentrations (T06H), respectively.

Fig. 2 Time-pressure cross sections of cloud ice (top), snow (middle) and graupel (bottom) mixing ratios for the TWP-ICE simulation T06L with the low ice crystal concentration.

Fig. 3 Same as Fig. 2 except for T06H with the high ice crystal concentration.

Fig. 4 Six-day mean vertical profiles of ice water content from the TWP-ICE observations and the three simulations using the low (T06L), moderate (T06M) and high ice crystal concentrations (T06H), respectively.

Figure 5 Vertical distributions of radar reflectivity from KWAJEX observations and two simulations. Blue, red and green symbols denote the observations and simulations K3DL and K3DN with the low and high ice crystal concentrations, respectively. Hollow and solid symbols represent mean and maximum radar reflectivity, respectively.

Fig. 6 Twenty-day mean vertical profiles of ice water content from the ARM-SGP observations and the three simulations using the low (A00L), moderate (A00M) and high ice crystal concentrations (A00H), respectively.

Fig. 7 Ice crystal concentration versus air temperature used in simulations T06L (thin solid), T06H (dashed) and T06Hu (thick solid line).

Fig. 8 Same as Fig. 2 except for T06Hu.

Fig. 9 Time-pressure cross sections of the retrieved ice water content over the Darwin station starting at 2100 UTC 6 February 2006.

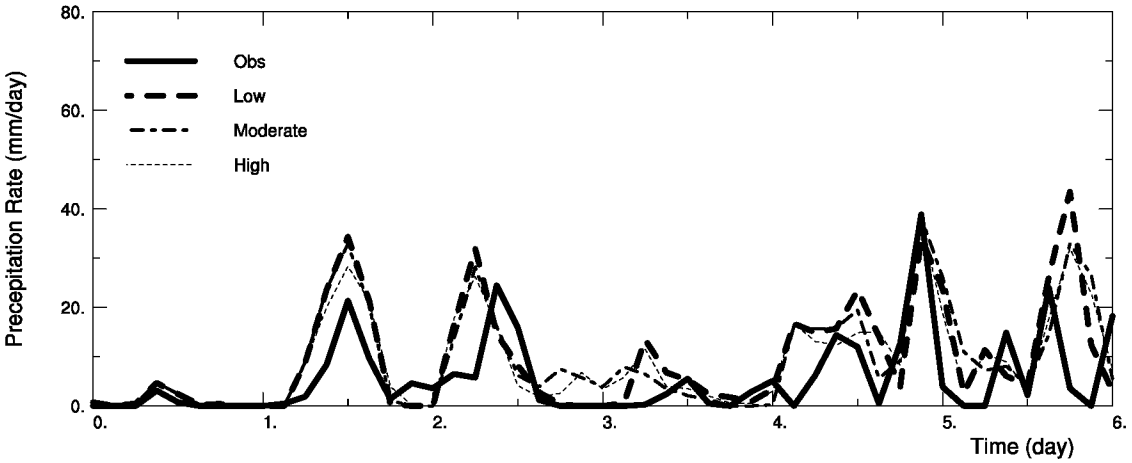

Fig. 1 Time series of surface precipitation rate for the TWP-ICE observations and three simulations that start at 2100 UTC 6 February 2006. Thick line represents the observations. Dashed, dot-dashed and dotted lines represent the modeling results with low (T06L), moderate (T06M) and high ice crystal concentrations (T06H), respectively.

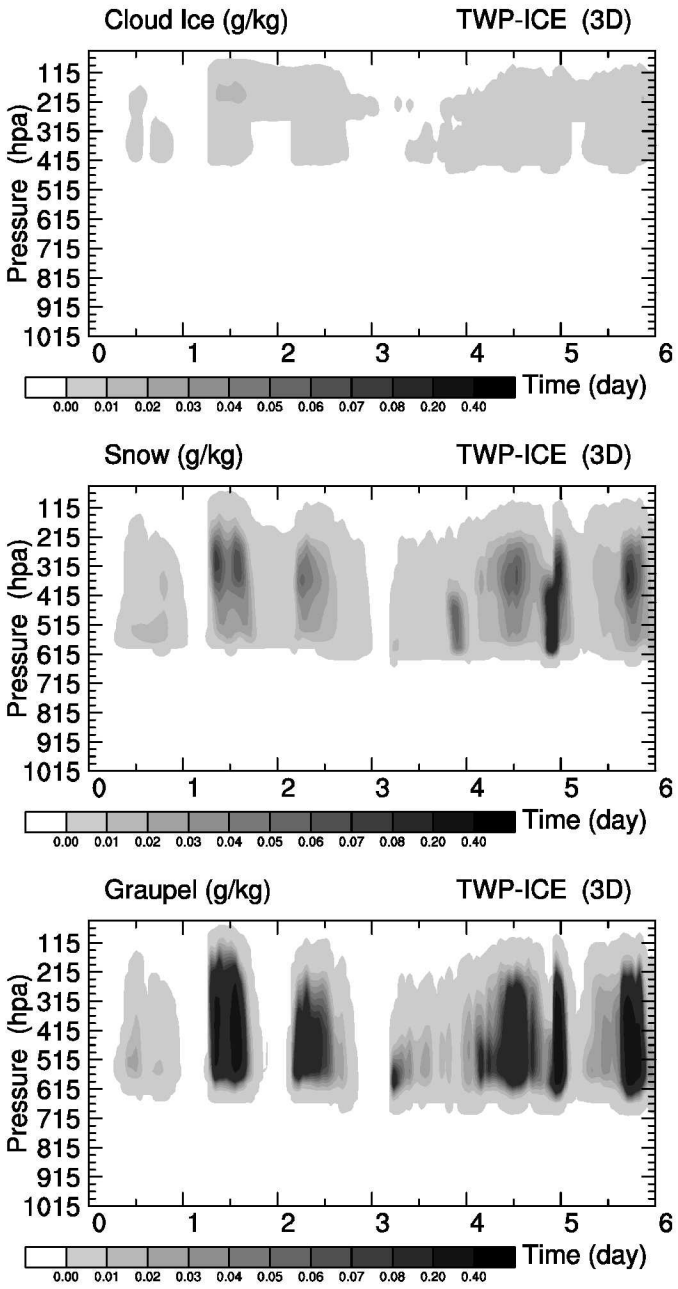

Fig. 2 Time-pressure cross sections of cloud ice (top), snow (middle) and graupel (bottom) mixing ratios for the TWP-ICE simulation T06L with the low ice crystal concentration.

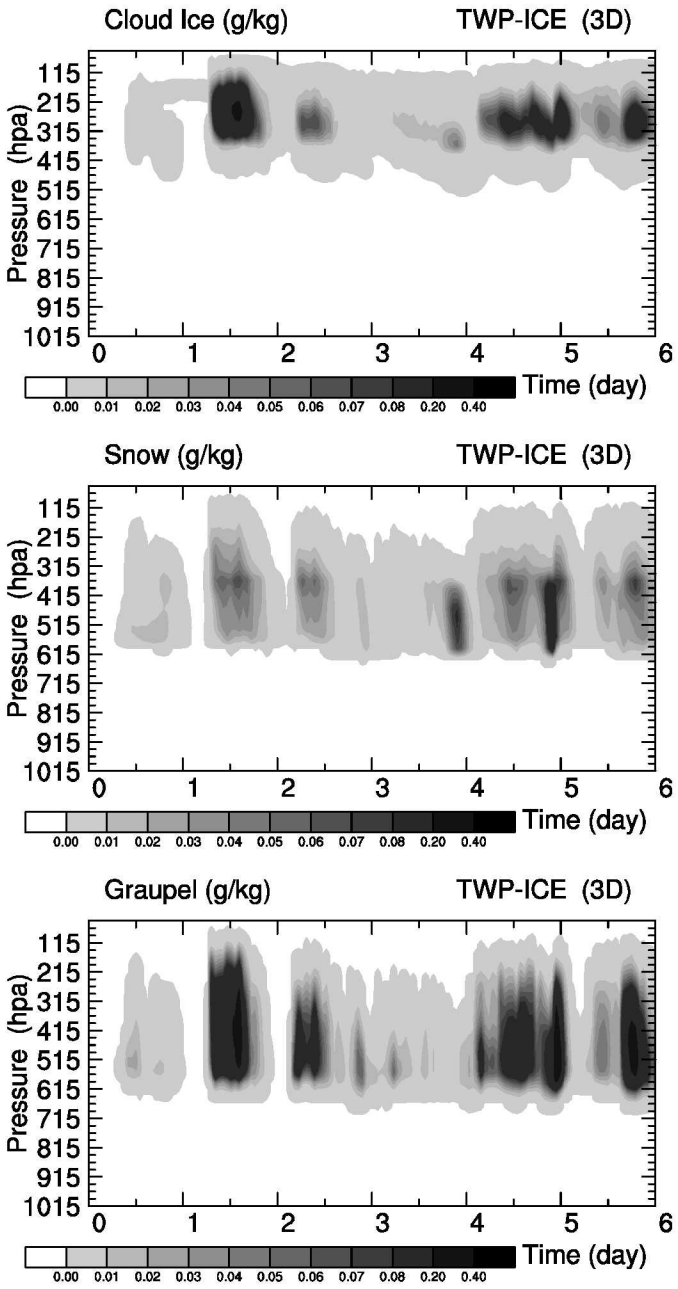

Fig. 3 Same as Fig. 2 except for T06H with the high ice crystal concentration.

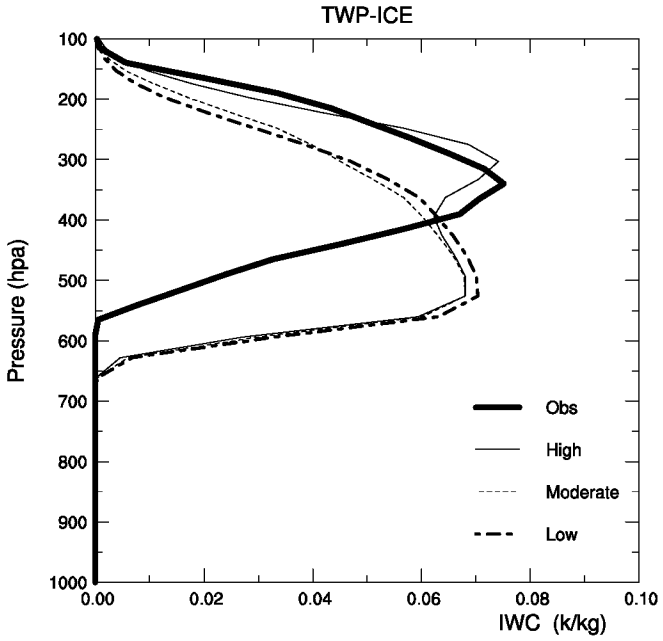

Fig. 4 Six-day mean vertical profiles of ice water content from the TWP-ICE observations and the three simulations using the low (T06L), moderate (T06M) and high ice crystal concentrations (T06H), respectively.

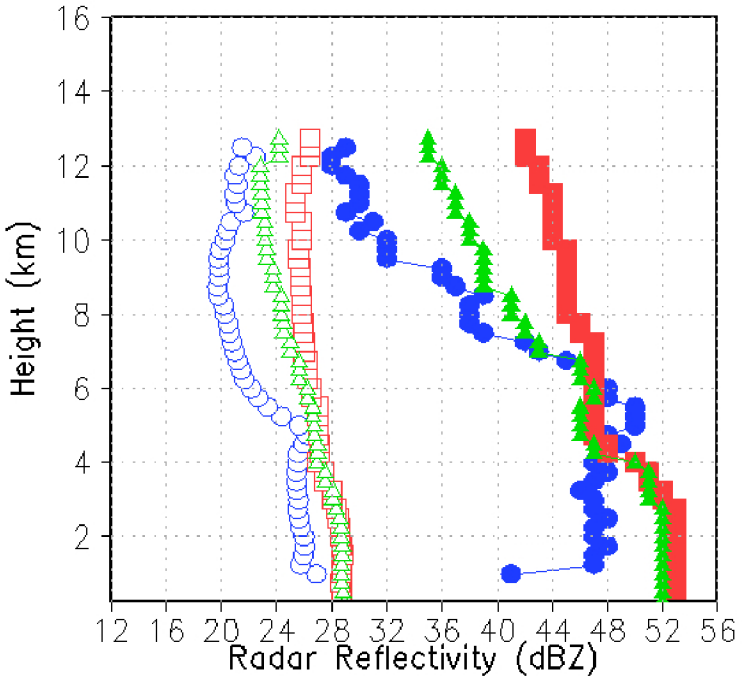

Figure 5 Vertical distributions of radar reflectivity from KWAJEX observations and two simulations. Blue, red and green symbols denote the observations and simulations K3DL and K3DN with the low and high ice crystal concentrations, respectively. Hollow and solid symbols represent mean and maximum radar reflectivity, respectively.

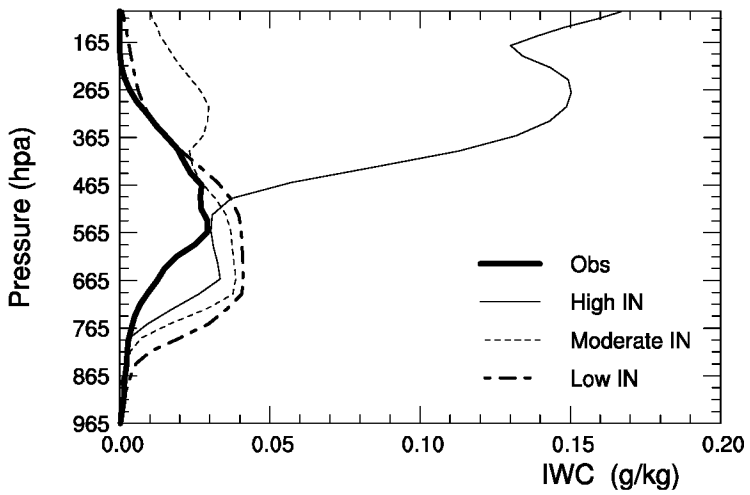

Fig. 6 Twenty-day mean vertical profiles of ice water content from the ARM-SGP observations and the three simulations using the low (A00L), moderate (A00M) and high ice crystal concentrations (A00H), respectively.

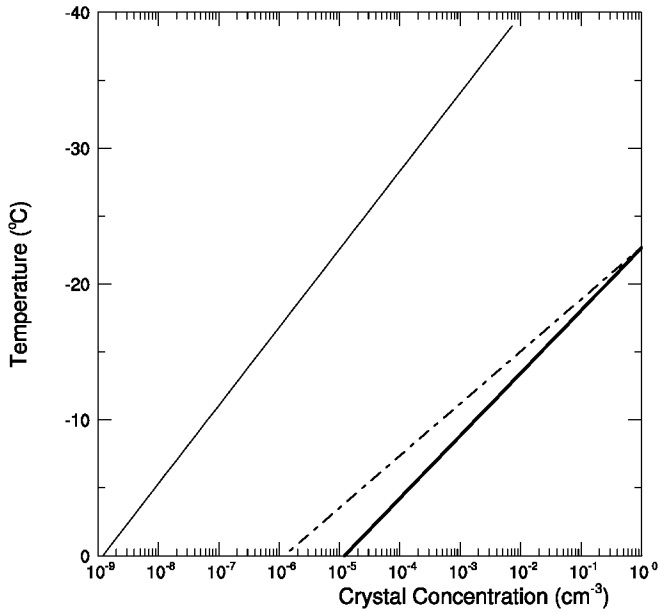

Fig. 7 Ice crystal concentration versus air temperature used in simulations T06L (thin solid), T06H (dashed) and T06Hu (thick solid line).

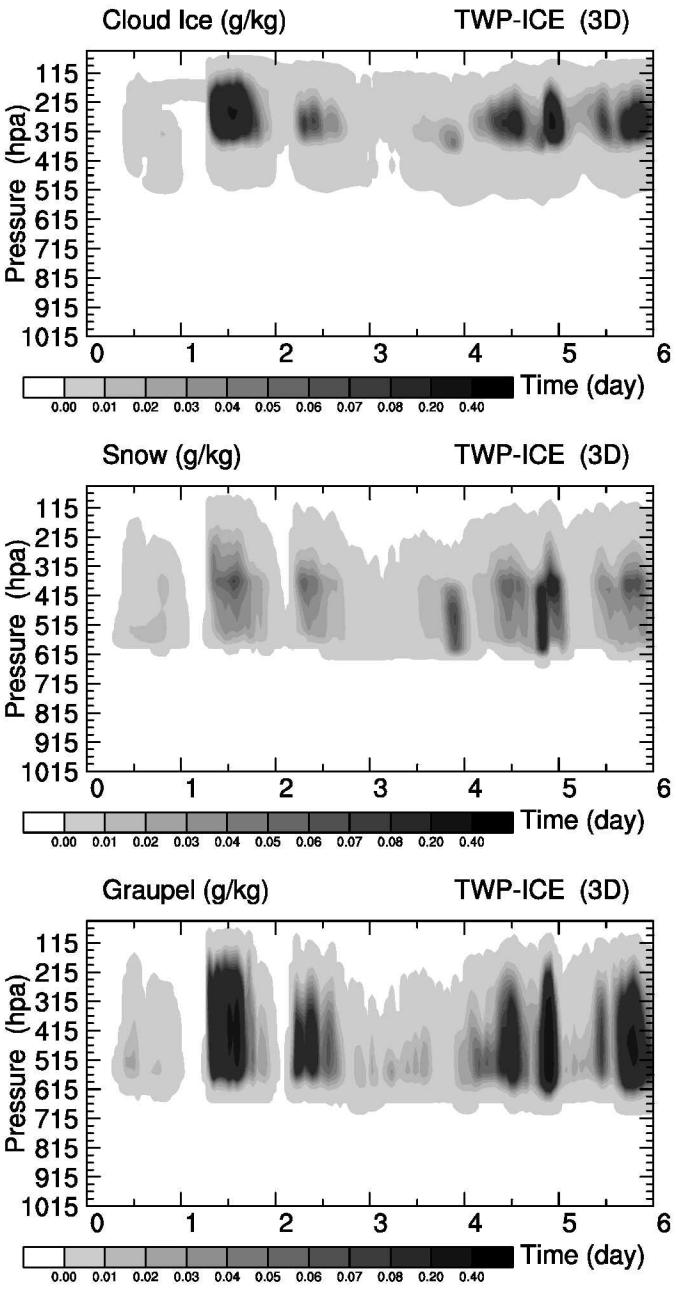

Fig. 8 Same as Fig. 2 except for T06Hu.

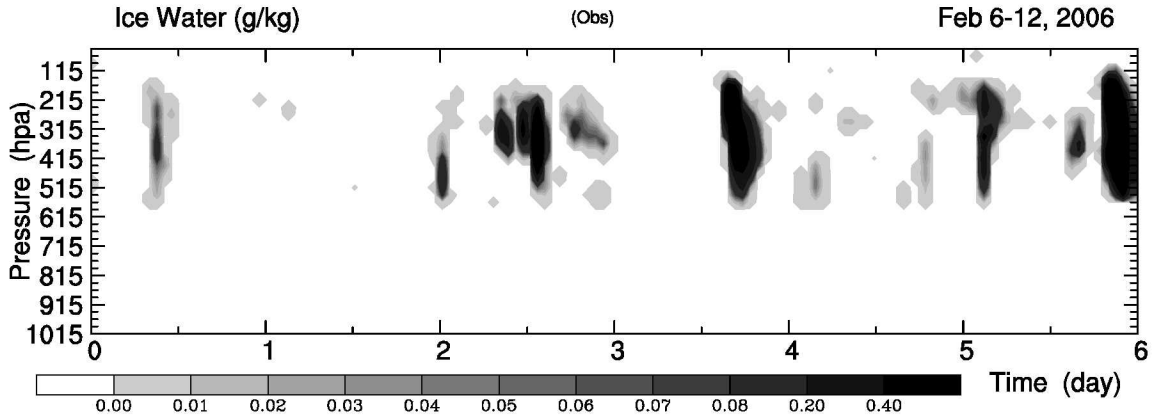

Fig. 9 Time-pressure cross sections of the retrieved ice water content over the Darwin station starting at 2100 UTC 6 February 2006.

Diagnosing the Ice Crystal Enhancement Factor in the Tropics

Xiping Zeng[1,2], Wei-Kuo Tao[2], Toshihisa Matsui[1,2], Shaocheng Xie[3], Stephen Lang[2,4], Minghua Zhang[5], David O'C Starr[2], Xiaowen Li[1,2], and Joanne Simpson[2]

[1]Goddard Earth Sciences and Technology Center, University of Maryland at Baltimore County, Baltimore, Maryland

[2]Laboratory for Atmospheres, NASA Goddard Space Flight Center, Greenbelt, Maryland

[3]Atmospheric Sciences Division, Lawrence Livermore National Laboratory, Livermore, California

[4]Science Systems and Applications Inc., Lanham, Maryland

[5]School of Marine and Atmospheric Sciences, Stony Brook University, New York

Popular Summary

Previous modeling studies have revealed that ice crystal number concentration is one of the dominant factors in the effect of clouds on radiation. Since the ice crystal enhancement factor and ice nuclei concentration determine the concentration, they are both important in quantifying the contribution of increased ice nuclei to global warming.

In this study, long-term cloud-resolving model (CRM) simulations are compared with field observations to estimate the ice crystal enhancement factor in tropical and mid-latitudinal clouds, respectively. It is found that the factor in tropical clouds is ~10^3-10^4 times larger than that of mid-latitudinal ones, which makes physical sense because entrainment and detrainment in the Tropics are much stronger than in middle latitudes.

The effect of entrainment/detrainment on the enhancement factor, especially in tropical clouds, suggests that cloud microphysical parameterizations should be coupled with subgrid turbulence parameterizations within CRMs to obtain a more accurate depiction of cloud-radiative forcing.